Original Research Paper

Optical and Structure Analysis of ZnO:Al Film

[1,2]Neilo Marcos Trindade, [3]Michel Chaves, [3]José Roberto Ribeiro Bortoleto,
[4]Américo Sheitiro Tabata and [4]José Humberto Dias da Silva

[1]*Departament of Physics, Federal Institute of Education, Science and Technology of São Paulo - IFSP, São Paulo, Brazil*
[2]*Institute of Physics, University of São Paulo - USP, São Paulo, Brazil*
[3]*Science and Technology Institute, São Paulo State University-UNESP, Sorocaba, SP, Brazil*
[4]*Departament of Physics, São Paulo State University -UNESP, Bauru, SP, Brazil*

Abstract: ZnO and ZnO:Al are wide-bandgap semiconductors which have many applications, mainly as transparent conducting films. Thin films of these compounds were deposited onto glass and silicon substrates by RF magnetron sputtering for the investigation of structural and optical characteristics. The XRD results show that the films present wurtzite structure. The formation of a polycrystalline film having a preferential crystallographic orientation in the plane (002) is observed in the doped samples. The Al incorporated films exhibited optical transmittance above 80% in the visible spectrum and a clear absorption band in the infrared due to free carriers. Additionally, the optical band gap around 3.48 eV is significantly above the values for the intrinsic ZnO (3.25 eV). Photoluminescence (PL) measurements showed a broad emission band in the visible region. In addition, PL emission lines at 3.32 and 3.37 eV showed up in Al incorporated films, and were related to excitonic emissions. The results show that the Burstein-Moss effect plays a central role in determining the optical characteristics of the doped material.

Keywords: Zinc Oxide, AZO, Burstein-Moss

Introduction

Films produced from doped metal oxides can have an excellent combination of optical transparency and electrical conductivity. These materials, called Transparent Conducting Oxides (TCOs), are fundamental components in different optoelectronic devices due to the ability to couple an optical transmittance of around 80% in the visible region and low electrical resistivity around 10^{-3} to 10^{-4} Ω.cm (da Silva *et al*., 2014). Recently, the TCOs films have attracted scientific and technological interest because of their potential application in illuminated panels, solar cells (Park *et al*., 2001; Alia *et al*., 2005); optical windows in residential, automotive (Sundaram and Khan, 1997) and gas sensors (Sahu and Huang, 2006). From a commercial standpoint, the most widely used has been indium tin oxide (In_2O_3:Sn), commonly known as ITO, especially in applications of various types of Liquid Crystal Displays (LCD) (Minami, 2008). However, due to the scarcity of indium, ITO generates a high production cost (Klingshirn, 2007). ZnO is one of the most promising candidates to replace ITO because of its low toxicity, availability and low production cost. It can also be produced on a large scale and presents high stability in the hydrogen plasma and thermal cycles used in the production device (Sahu and Huang, 2006; Das and Ray, 2003; Lin *et al*., 2011; Tohsophon *et al*., 2011).

There are several articles reporting advances in the synthesis and application of semiconductor thin films based on ZnO with great potential for the replacement of ITO, in addition to optoelectronics applications (Pla *et al*., 2003; Ong *et al*., 2005), such as Organic Light Emitting Diodes (OLED), transistors, solar cells and non-volatile memories (Song *et al*., 2013). In particular, as solar cells, it has grown into application areas that need low-power, for example, those related to telecommunications, maritime signaling and land, rural electrification, etc. (Lunas, 2009). The quality of the solar cells strongly depends on the quality of the TCO films, requiring rough surfaces and resistivity in the range of $1\text{-}5\times10^{-4}$ Ω.cm and good optical properties (Tohsophon *et al*., 2011). Other applications include ZnO acoustic wave devices (Melloch and Wagers, 1983), heat reflectors (Das and Ray, 2003) and gas sensors (Ushio *et al*., 1994). In the ultraviolet spectral range, ZnO has also been used as an emitting material in the blue band in the visible (Bixia *et al*., 2001).

To reduce the electrical resistivity of this material different types of dopants have been used in Groups III and IV, such as B, Ge, Ti, Al, Ga, In, rare earth (Ferreira,

2008). The Al^{3+} ions (0.54 Å) and Ga^{3+} (0.62 Å) are considered the best dopants because they have ionic radii close to the radius of the ion Zn^{2+} (0.74 Å) (Ferreira, 2008). The doping of ZnO by Al atoms occurs by substitution of an Al atom by a Zn atom in its hexagonal lattice. It can also be done by migration of Al to a non-crystalline region of the grain boundaries, forming links between Al-O. Most of these atoms can replace Zn^{2+} by ionizing to Al^{3+}. Thus, the aluminum atoms play important role in the crystal lattice, acting as substitutes ions. Consequently, a free electron is likely to be present for each substitutional of Al atom (Yu *et al.*, 2005).

As a conductive transparent oxide, ZnO doped with Al [also found in the literature as AZO (Al-doped ZnO)] shows great promise for applications such as emitters in the range UV/blue, photodetectors, and transparent electronics (Bixia *et al.*, 2001). Applications such as solar cells had already been reported in the 90's using zinc oxide doped with aluminum with properties superior to zinc oxide doped with indium in terms of resistivity and transparency (Harding *et al.*, 1991; Martínez *et al.*, 1997). Later, its chemical (Yoo *et al.*, 2005) and thermal stability differential during processing (Mosbah and Aida, 2012) was also reported. Other features, which promote its use, are its constituents Zn and Al, which are more abundant and less toxic than the constituents of ITO (Klingshirn, 2007).

In the present investigation the main objective was to compare the structural and optical properties of transparent and conductive films of ZnO and ZnO:Al. This study also sought to identify the conse-quences of the Burstein-Moss effect in the analyzed TCOs, in particular in relation to optical bandgap.

Materials and Methods

The synthesis of ZnO and ZnO:Al thin films used disc-shaped Zn and ZnAl metallic targets, 99.99% purity, with diameters of 75 mm and 2 mm thickness. The deposition system consists of a cylindrical 304 stainless steel chamber of 270 mm diameter and 200 mm in height. The partial pressure of oxygen and argon were set at a ratio of 1:10. The total pressure was kept at 10 mTorr, and the depositions lasted 20 minutes. Films were deposited on 1mm-thick glass substrates by RF magnetron sputtering with the plasma source maintained at a frequency of 13.56 MHz (RF) and power of 100 W. A substrate tem-perature of 373K was maintained during the growth. In order to produce ZnO:Al, the target composition consisted of 98 wt.% zinc and 2 wt.% aluminum. The choice of 2 wt.% Al doping of ZnO was due to studies reported by other authors (Das and Ray, 2003; Mosbah and Aida, 2012; Kwak, 2004; Dao *et al.*, 2009), regarding this composition as the best condition for a low resistivity (ρ ~ 10^{-4} Ω.cm) for this type of film. Glass (25×40 mm) and (001) silicon (100 mm²)

substrates were cleaned using detergent (Det Limp S32), deionized water and isopropyl alcohol in ultrasound baths before loading onto the sample holder.

The measurements of X-Ray Diffraction (XRD) were performed employing an X-ray diffractometer (PanalyticalX'Pert Powder) with CuK_α radiation wavelength equals 1.5405 Å, allowing the identification of the structure, the crystal orientation and average crystallite size. The geometry used was 2 theta (grazing angle) and a scanning speed of 0.01° s^{-1} at an incident angle of 2° and the scanning range was 20-90°. By using the XRD data, one can estimate the values of the crystallite size by the Scherrer equation (Jiang *et al.*, 2009; Chaves *et al.*, 2013):

$$\chi = \frac{0.9\lambda}{\beta \cos\theta}$$

where, λ, θ and β are respectively the wavelength of the X-ray Bragg angle related to study diffraction peak and the half width of this peak.

Optical transmittance and reflectance technique UV-Vis-NIR was used in the optical characterization. The optical transmittance spectra were measured in a Perkin Elmer Lambda 1050 spectrophotometer. The investigated range was 250 to 2500 nm with a resolution of 0.05 nm in the visible region and 0.2 nm in the infrared region. The transmittance and reflectance spectra data were treated in a computational routine based on Cisneros method (Cisneros, 1998), which allowed the calculations of sample thickness, refractive index, extinction and absorption coefficients. The optical band gap of the materials was used by the following recurrent expression for direct band gap semiconductors (Pankove, 1971; Yu and Cardona, 2010):

$$ahv = A(hv - E_g)^{1\backslash 2}$$

Where:
a = The absorption coefficient
hv = The photon energy
E_g = The bandgap
A = A constant

A is related to the effective masses of electrons and holes, but in practice also reflects the crystallographic quality of the material (Pankove, 1971; Yu and Cardona, 2010).

Photoluminescence (PL) spectroscopy was carried out at 10K, by using a cold finger cryostat cooled by helium flow. The excitation source of the samples was provided by the 325 nm line of a Kimmon Helium-Cadmium laser. A Spex 1780 monocromator (controlled by a PC) with a diffraction grating of 600 gr/mm and blaze of 1.0 μm was used to collect the PL signal. A

Peltier cooled RCA GaAs photo-multiplier mounted at the exit slit of the monochromator detected the signal after optical dispersion. A digital Keithley 617 electrometer was used to read the signal and to send it to a PC. The laser line was focalized in the sample´s surfaces and the PL emission was collected by a lens and focalized at the entrance slit of the monochromator.

Results and Discussion

At room temperature ZnO is found in the wurtzite structure, which is thermodynamically more stable (Peres, 2007). The unit cell has two external lattice parameters: the basal plane (a) and uniaxial plane (c) and an internal parameter *u*, which describes the cation and anion positions relative to the *z* axis (Jaffe and Hess, 1993; Marana *et al.*, 2008). The ZnO wurtzite structure belongs to the space group P63mc with a Bravais lattice (*a* = 3.250 Å and *c* = 5.207 Å and internal coordinate *u* = 0.382) (Decremps *et al.*, 2003) and can be depicted as a zinc atom surrounded by four oxygen atoms with sp^3-hybridization in a tetrahedron configuration along the c-axis. In the ZnO this value is close to a hexagonal cell with a notional value of the c/a ratio of 1.633 (Morkoç and Özgür, 2009).

The samples showed the formation of a polycrystalline film having a preferential crystallographic orientation in the plane (002), shown in Fig. 1. This indicates that the orientation film grows along c-axis, the direction [001] and perpendicular to the substrate surface (Zhang *et al.*, 2002; Kuchiyama *et al.*, 2011; Tang *et al.*, 2013).

This growth characteristic along the c-axis is associated with the lowest free energy referred to the plan (002) (Fujimura *et al.*, 1993). In the first stage of growth of the film, certain grains with particular orientation start growing; coalescence and thermodynamic orientation of the c-axis are achieved (Park *et al.*, 1997).

The ZnO and ZnO:Al films in addition to presenting a preferential peak in the plane (002) also exhibit the presence of the planes (100), (101), (102), (110) and (103), indicating that there was little formation of crystalline structure in other crystallographic directions of ZnO. The XRD results show that Al doped ZnO does not alter the structural characteristics, since the most intense peaks of the doped sample show up in positions very close to the ones noticed in undoped samples. The Bragg angles, intensities, full width at half maximum (FWHM) and crystallite size estimated using Scherrer´s formula for the (002) planes of the samples are listed in Table 1.

The results of the Table 1 show that there is a variation ~ 0.8° at the peak position (002) between the pure sample and the doped sample with Al, a consequence of decrease in the lattice parameter c, This change in position is due to the difference between the ionic radius of Zn^{2+} (0.74 Å) and Al^{3+} (0.54 Å), causing tensions that consequently change the lattice parameters, indicating that the Al atoms replace Zn sites (Jiang *et al.*, 2009; Park *et al.*, 1997; Ellmer *et al.*, 2007; Lin *et al.*, 2010).

It is observed in doped sample with Al that the peak is more intense and the FWHM has a lower value when compared to the pure sample. Therefore, this indicates an improved crystallinity and, for the same preparation conditions, the crystallite size of the ZnO: Al is bigger than that of ZnO (Ma *et al.*, 1996). The FWHM of the peak (002) was used to estimate the average size of crystallite along the c-axis by the Scherrer equ-ation. The results show that there is an increase in crystallite size when comparing doped (~14 nm) with the undoped sample (~10 nm). The value of stresses is calculated using equation based on the lattice parameter and is negative because are tensile in a direction of the c-axis. The increase in stress is expected in doped films since the presence of dopant atoms causes an increase in crystal lattice disorder. During the growth of the film this disorder is also generated due to defects, known with intrinsic stress. These deformations increase the energy gap in the case of compressions (Dimova-Malinovska *et al.*, 2008). We observed that there is an increase in the size of the crystallite accompanied by an increase in stress under the same growth conditions, but because it is two samples, further investigation is necessary.

The dependence of spectral transmittance and refletance of the ZnO and ZnO:Al deposited on a glass substrate is shown in Fig. 2. Firstly, the values of the thickness and refractive index for the samples were calculated from the transmittance and reflectance data for λ = 550 nm by the Cisneros method (Cisneros, 1998). The results are shown in Table 2. The obtained values of thickness show that the films presented nanometric character. There is no significant correlation between the refractive index of the doped and pure sample.

A transmittance above 80% can be observed in the visible spectral region for all films.

In the range below the wavelength around 400 nm corresponds to energies greater than or equal to the energy value of the band gap. The strong absorption observed in the near ultraviolet region is typical of interband transition (valence-conduction) in broadband semiconductors. In the visible range, the high transmittance is related to the lack of allowed interband transitions and to frequencies much higher than the plasma frequency of the free carriers. However, a gradual decrease in transmittance can be observed in the infrared region, which is related to the metallic character of the free electrons in the conduction band (Nsimama and Samiji, 2012).
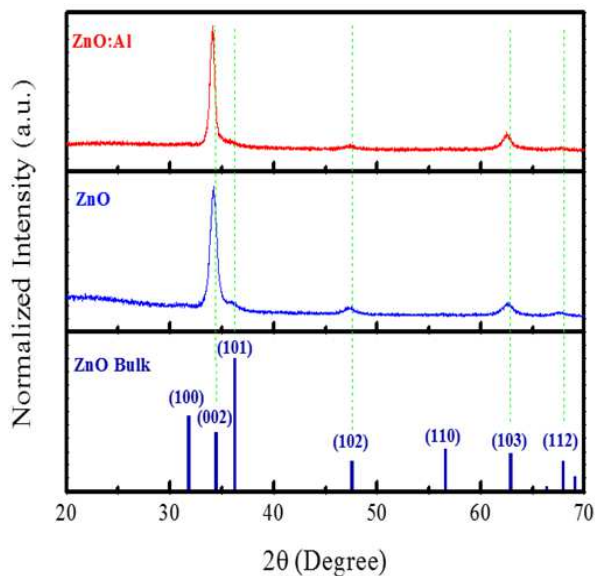
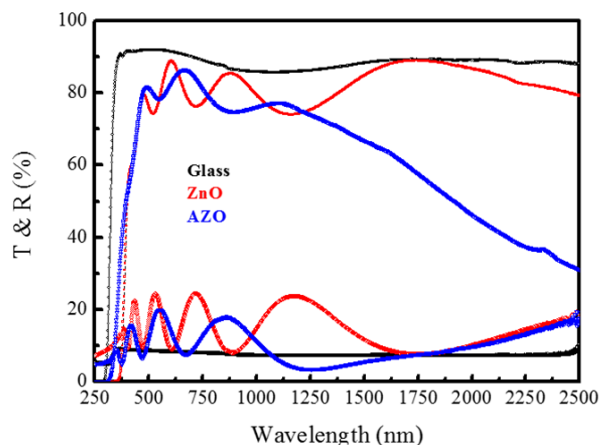Fig. 1. XRD patterns of the ZnO and ZnO:Al films deposited onto glass substrates

Fig. 2. Optical transmittance (a) and reflectance (b) of glass substrate and films obtained

Table 1. Measurements of the peak (002) angle, intensity, FWHM, and crystallite size

Sample	Peak (002) 2θ (°)	Intensity (002) (cps)	FWHM (002) (°)	Crystallite Size (nm)	Lattice Parameter c (nm)	Stress σ (GPa)
ZnO Undoped	34.1948	1587	0.8118	10.2	0.5240	-1.47
ZnO:Al	34.0814	2943	0.5877	14.13	0.5256	-2.19
JCPDS 36-1451	34.42				0.5207	

Table 2. Values of the thickness and refractive index for the samples, calculated from the transmit-tance and reflectance data for λ = 550 nm by the Cisneros method (Cisneros, 1998)

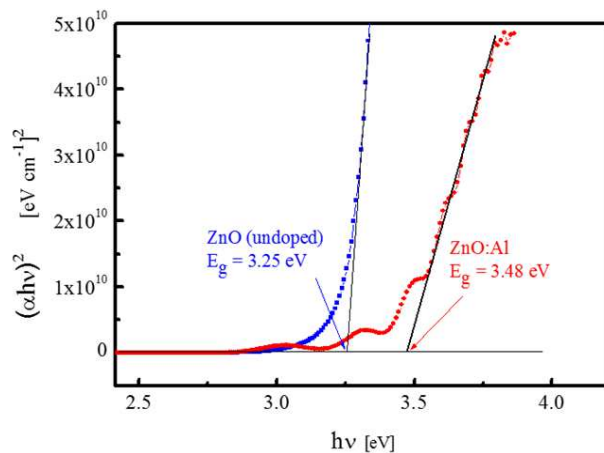| Sample	Substract refractive index (u.a.)	Film refractive index (u.a.)	Thickness (nm)
ZnO	1.58	2.02	454
ZnO:Al	1.54	1.93	367

Fig. 3. Absorption edges of ZnO and ZnO:Al samples, calculated using the procedure for direct bandgap materials.

The classical free electron Drude model can be used, together with the spectral response, to estimate the carrier concentration on the conduction band. In the context of this model, the plasma frequency (ω_p) divides the spectrum in highly reflecting and low transmitting (frequencies smaller than ω_p) and low reflecting and transparent (frequencies bigger than ω_p). In the Drude model ω_p is proportional to the square root of the carrier concentration (Rahmane et al., 2015), so it can explain the increase in T at higher frequencies if the carrier concentration is sufficiently low. In quantum mechanical terms, the electronic oscillations provided described by the classical model are equivalent to intraband transitions of electrons in the conduction band. So, the transmittance window in the visible range is limited by interband transitions at higher energies and intraband transitions at lower energies.

The effect of conduction band filling by free electrons can be noted on the absorption edge. Fig. 3 shows the bandgap determination plots for the undoped and Al doped films, where bandgap shift due to doping is clear. The absorption coefficients were calculated using the transmittance of the films and substrates and the Cisneros procedure method for thin films onto weakly absorbing substrates.

For ZnO films doped with aluminum, values of the optical band gaps in the 3.50 eV energy range were obtained above the intrinsic ZnO ones. The displacement of the energy of the optical gap is associated with the Burstein-Moss effect presented by Burstein (1954) (Burstein, 1954). According to the literature (Lu and Fujita, 2007), in heavily doped n-type semiconductors electrons occupy states at the bottom of the conduction band and Fermi energy moves into the conduction band. Due to the excursion of Fermi level, optical interband transitions can only occur to photons that can make

vertical transitions from the valence band to a state above the Fermi energy in the conduction band (Lu and Fujita, 2007). Therefore, the optical absorption edge shifts to higher energy and the optical energy gap increases. In the infrared region, the doped sample showed a high extinction coefficient in relation the pure sample, this indicates that there is a greater quantity of carriers present in the conduction band influenced by the presence of Al in films, and hence, promoting the occurrence of the Burstein-Moss effect.

The fringes of low energy interference in the curve of the absorption coefficient for the doped film may be related to defects created by the presence of aluminum and investigated by photoluminescence. The photoluminescence spectra of the ZnO and ZnO:Al films measured at 10 K are displayed in Fig. 4. In the pure compound, a broad visible band with a weak tail to UV is observed. The PL emission related to the Al incorporated sample display a slightly different line shape in the visible, and a clear pair of narrow bands in the UV (Fig. 4, red curve).

Generally, ZnO emission bands can be separated into two parts: (i) UV exciton bands and (ii) visible defect bands. The exact origin of the defect emission band in ZnO is not well understood and has been the subject of various interpretations, such as oxygen vacancies, zinc interstices, Zn antisites, extrinsic impurities and complex defects (Bixia *et al*., 2001; Martins, 2012; Das and Mondal, 2014). Previous reports indicate that the radiative lifetime of ex-citons pure ZnO is in the nanosecond range, while in the visible range the lifetime of the emission is longer, i.e., in the range of microseconds, so this justifies the emission is stronger in the visible (Das and Mondal, 2014). However, the complex dependence of UV and visible emission intensities is still subject of controversy in the literature (Mohanta, 2014; Manzano *et al*., 2011; Khan *et al*., 2013).

The UV band emission is dominated by excitonic transitions (Bixia *et al*., 2001; Das and Mondal, 2014). According to Das and Mondal (2014) the appearance of the band around 3.35 eV is related to exciton emission or emission qua-si-band, that is, the photo-excited electrons recombine with holes in the valence band or traps near the valence band, considering that this is a value below the gap for pure ZnO.

In the UV range the emission lines showed the highest intensity around 3.32 eV and 3.37 eV (Fig. 4). The emission line at 3.32 eV occurs in a spectral region where the appearance is expected emissions related to Two Electrons Satellites (TES) exciton bound donors (Djurisic and Leung, 2006; Meyer *et al*., 2004). The emission line in the range of 3.37 to 3.35 eV is correlated emissions bounded excitons (Klingshirn, 2007) and by restricting the range of 3.37 to 3.36 eV these excitons are linked to donor atoms (D^+X, D^0X).
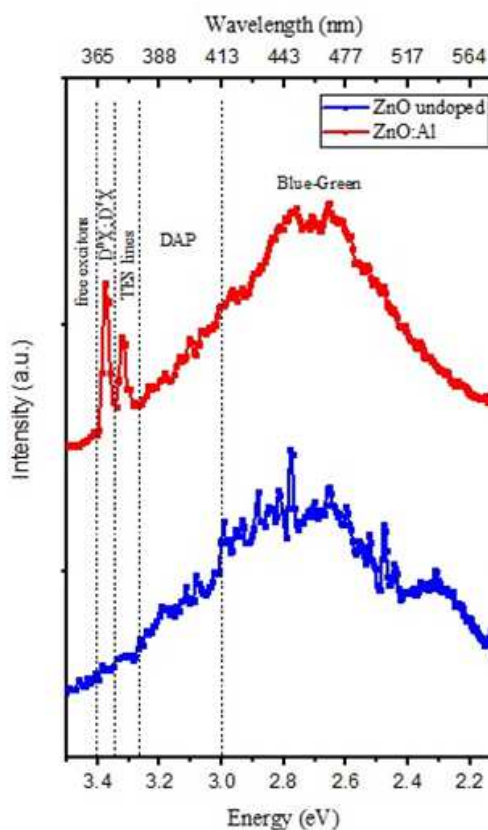

Fig. 4. Photoluminescence of ZnO and ZnO:Al samples deposited on the silicon substrate, at tem-perature 10K with excitation source λ = 325 nm
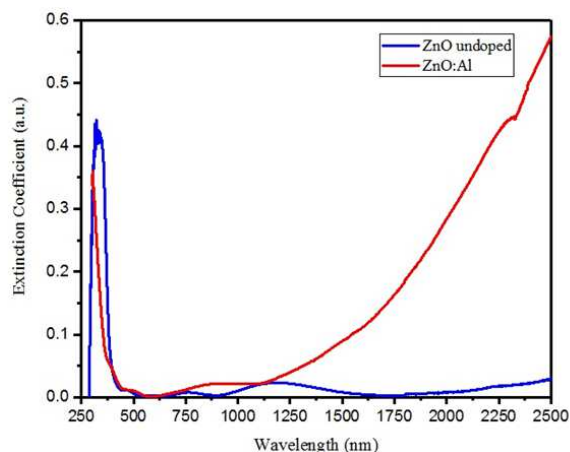

Fig. 5. Variation of the extinction coefficient versus wavelength measurements of ZnO and ZnO: Al

The chemical identification of these donors is still unclear (Djurisic and Leung, 2006). Both emission lines present in the PL spectra of our samples; 3.32 eV (Meyer *et al*., 2004) and 3.37 eV (Peres, 2007) suggest a correlation with the effect of doping Al; since they are not present in the pure sample spectrum.

794

Concerning the visible PL emission, Lin *et al.* (2001) observed the green emission centered at 2.38 eV of the ZnO film deposited on silicon substrates and suggest that the green emission should correspond to the passage of electrons from the bottom of the conduction band for the level of antisite defects. Recently, ZnO spectrum was characterized by a green emission band that was associated with a defect level of oxygen vacancy (Mohanta, 2014). Also according to Wang *et al.* (2011) ZnO displays two bands centered at 510-540 nm (green emission) and 600-640 nm (yellow emission), assigned to oxygen vacancy (V_o) and interstitial oxygen (O_i), respectively.

According to Das and Mondal (2014), the visible PL emissions from pure ZnO films prepared by magnetron sputtering, correspond to a broadband coming from a convolution of different transitions that are related to the oxygen vacancy states, Zn interstitial, doubly ionized Zn vacancy and oxygen antisite.Due to the different assignments found to the sub-bands of the visible PL emission, it was not possible to attribute a single set of contributions to the observed signal. The difficulty in identifying the origins of emissions-related defects is due to the complexity of microscopic details involved (Das and Mondal, 2014). So, we would rather let them generically attributed to the different kinds of defects, while the narrow UV bands were attributed to Two Electrons Satellites (TES) and excitons are linked to donor atoms (D^+X, D^0X).

To complement the results, Fig. 5 shows the extinction coefficient values for the deposited films.

It is observed that the extinction coefficient for the doped and the undoped samples no more than 0.05 to the visible spectrum, with typical extinction coefficients of transparent films. In the infrared region, the doped sample showed a high extinction coefficient before the pure sample, which maintains a value around zero in this range, this indicates that there is a greater quantity of carriers present in the conduction band influenced by the presence of Al in films, and hence, promoting the occurrence of the Burstein-Moss effect.

Conclusion

Polycrystalline ZnO and ZnO:Al films were produced (20 min deposition) by RF reactive sputtering using Zn and ZnAl targets and Ar and O_2 gas mixtures. The crystallites presented wurtzite structure and a high degree of orientation texture, being the crystallites c-axis preferentially oriented perpendicular to the surfaces of the substrates. The Al incorporation (2 wt.%) has produced significant increases in orientation texture and crystallite sizes. The optical band gap values of the Al incorporated samples are in the range 3.48 eV that are

above the values obtained for ZnO intrinsic (3.25 eV). The Al incorporation results in two clear PL excitonic bands in the UV and are in qualitative agreement with the results obtained in the optical absorption coefficient. The extinction coefficient showed a high absorption in the infrared region doped samples compared to the undoped sample, and therefore, confirmed the increased carrier density by doping presence. The optical results show *Burstein-Moss* as the dominant effect related to Al incorporation in the films.

Acknowledgement

Author's Contributions

All the authors contributed equally to prepare, develop and carry out this manuscript.

Ethics

Authors declare that are not ethical issues that may arise after the publication of this manuscript. This manuscript contains unpublished material.

References

Alia, H.M., H.A. Mohamed and S.H. Mohamed, 2005. Enhancement of the optical and electrical properties of ITO thin films deposited by electron beam evaporation technique. Eur. Physical J. Applied Physics, 31: 87-93. DOI: 10.1051/epjap:2005044

Bixia, L., F. Zhuxi and J. Yunbo, 2001. Green luminescent center in undoped zinc oxide films deposited on silicon substrates. Applied Physics Lett., 79: 943-945. DOI: 10.1063/1.1394173

Burstein, E., 1954. Anomalous optical absorption limit in InSb. Physical Rev., 93: 632-633. DOI: 10.1103/PhysRev.93.632

Chaves, M., E.P. da Silva, S.F. Durrant, N.C. da Cruz and P.N. Lisboa-Filho *et al.*, 2013. Effect of Zn sputtering rate on the morphological and optical properties of ZnO films. Mater. Sci. Applic., 4: 802-807. DOI: 10.4236/msa.2013.412102

Cisneros, J.I., 1998. Optical characterization of dielectric and semiconductor thin films by use of transmission data. Applied Optics., 37: 5262. DOI: 10.1364/AO.37.005262

da SilvaI, É.P., M. ChavesI, S.F. DurrantI, P.N. Lisboa-FilhoII, J.R.R. BortoletoI *et al*., 2014. Morphological and electrical evolution of ZnO:Al thin films deposited by RF magnetron sputtering onto glass substrates. Materials Res., 17: 1384-1390. DOI: 10.1590/1516-1439.281214

Dao, V.A., T. Le, T. Tran, H.C. Nguyen and K. Kim *et al*., 2009. Electrical and optical studies of transparent conducting ZnO:Al thin films by magnetron dc sputtering. J. Electroceram, 23: 356-360. DOI: 10.1007/s10832-008-9466-6

Das, D. and P. Mondal, 2014. Photoluminescence phenomena prevailing in c-axis oriented intrinsic ZnO thin films prepared by RF magnetron sputtering. RSC Advances, 4: 35735-35743. DOI: 10.1039/C4RA06063F

Das, R. and S. Ray, 2003. Zinc oxide- a transparent conducting IR-reflector prepared by rf-magnetron sputtering. J. Phys. D.: Appl. Phys., 36: 152-155.

Decremps F., F. Datchi, A.M. Saitta, A.Polian and S. Pascarelli *et al*., 2003. Local structure of condensed zinc oxide. Physical Review B. 68: 1098-1121. DOI: 10.1103/PhysRevB.68.104101

Dimova-Malinovska, D., H. Nichev and O. Angelov, 2008. Correlation between the stress in ZnO thin film and Urbach band trail width. Current Topic Solid State Physics, 10: 3353-3357. DOI: 10.1002/pssc.200778886

Djurisic, A.B. and Y.H. Leung, 2006. Optical properties of ZnO nanostructures. Small, 2: 944-961. DOI: 10.1002/smll.200600134

Ellmer, K., A. Klein and B. Rech, 2007. Transparent Conductive Zinc-Oxide: Basics and Applications in Thin Film Solar Cells. 1st Edn., Springer-Verlag, Berlin, pp: 446. ISBN-10: 3540736123

Ferreira, N.S., 2008. Deposição e caracterização de filmes de óxido de zinco dopado com alumínio. [Dissertation]. Rio de Janeiro: Universidade Federal do Rio de Janeiro.

Fujimura, N., T. Nishihara, S. Goto, J. Xu and T. Ito, 1993. Control of preferred orientation for ZnO$_x$ films: Control of self-texture. J. Crystal Growth, 130: 269-279. DOI: 10.1016/0022-0248(93)90861-P

Harding, G.L., B. Window and E.C. Horrigan, 1991. Aluminium-and indium doped zinc oxide thin films prepared by DC magnetron reactive sputtering. Sol. Energy Mater. Sol. Cells, 22: 69-91. DOI: 10.1016/0165-1633(91)90007-8

Jaffe, J.E. and A.C. Hess, 1993. Hartree-Fock study of phase-changes in ZnO at high-pressure. Phys. Review B., 48: 176. DOI: 10.1103/PhysRevB.48.7903

Jiang, Y.J., D.X. Zhang, H.K. Cai, K. Tao and Y. Xue *et al*., 2009. Influence of the gas flow of Argon and the distance between substrate and plasma on properties of Al-doped zinc oxide films. J. Physics: Conference Series, 152: 1-7. DOI: 10.1088/1742-6596/152/1/012030

Khan, F., S. Ameen, M. Song and H.S. Shin, 2013. Influence of excitation wavelength on photoluminescence spectra of Al doped ZnO films. J. Luminescence, 134: 160-164. DOI: 10.1016/j.jlumin.2012.08.054

Klingshirn, C., 2007. ZnO: From basics towards applications. Phys. Stat. Sol., 244: 3027-3073. DOI: 10.1002/cphc.200700002

Kuchiyama, T., K. Yamamoto, S. Hasegawa and H. Asahi, 2011. Surface morphology and crystalline structure of high-stable polycrystalline transparent conductive zinc oxide films. Applied Surface Sci., 258: 1488-1490. DOI: 10.1016/j.apsusc.2011.09.112

Kwak, D.J., 2004. Argon gas pressure and substrate temperature dependences of ZnO:Al film by magnetron sputtering. J. Korean Physical Society, 45: 206-210.

Lin, B., Z. Fu and Y. Jia, 2001. Green luminescent center in undoped zinc oxide films deposited on silicon substrates. Applied Physics Lett., 79: 943-946. DOI: 10.1063/1.1394173

Lin, S.S. and D.K. Wu, 2010. The properties of Al-doped TiO$_2$ nanoceramic films deposited by simultaneous rf and dc magnetron sputtering. Ceramics Int., 36: 87-91. DOI: 10.1016/j.ceramint.2009.06.023

Lin, Y.C., B.L. Wang, W.T. Yen and C.H. Shen, 2011. Surface textured molybdenum doped zinc oxide thin films prepared for thin film solar cells using pulsed direct current magnetron sputtering. Thin Solid Films., 519: 5571-5576. DOI: 10.1016/j.tsf.2011.03.014

Lu, J.G. and S. Fujita, 2007. Carrier concentration dependence of band gap shift in n -type ZnO:Al films. J. Applied Physics, 101: 083705. DOI: 10.1063/1.2721374

Lunas, F.R., 2009. Caracterização de Filmes Finos de ZnO Dopados com Al e Mn Depositados em Substrato Vítreo pelo Método Spray Pirólise. [Dissertation]. São Paulo: Universidade Estadual Paulista.

Ma, J., F. Ji, H.L. Ma and S.Y. Li, 1996. Electrical and optical properties of ZnO: Al films prepared by an evaporation method. Thin Solid Films, 279: 213-215. DOI: 10.1016/0040-6090(95)08173-9

Manzano, C.V., O. Caballero-Calero, B. Alén and M.S. Martín-González, 2011. Synthesis and luminescence properties of eletrodeposited ZnO films. J. Applied Physics, 110: 043538. DOI: 10.1063/1.3622627

Marana, N.L., V.M. Longo, E. Longo, J.B.L. Martins and J.R. Sambrano *et al.*, 2008. Electronic and structural properties of the (1010) and (1120) ZnO surfaces. J. Phys. Chem. A, 112: 8958-8963. DOI: 10.1021/jp801718x

Martínez, M.A., J. Herrero and M.T. Gutiérrez, 1997. Deposition of transparent and conductive Al-doped ZnO thin films for photovoltaic solar cells. Sol. Energy Mater. Sol. Cells, 45: 75-86. DOI: 10.1016/S0927-0248(96)00066-9

Martins, R.J., 2012. Controle coerente das bandas de emissão de ZnO através de algoritmo genético. [Dissertation]. São Carlos: Universidade Federal de São Carlos.

Melloch, M.R. and R.S. Wagers, 1983. Propagation loss of the acoustic pseudosurface wave on (ZXt)45° GaAs. Appl. Phys. Lett. 43: 1008-1009. DOI: 10.1063/1.94224

Meyer, B.K., H. Alves, D.M. Hofmann, W. Kriegseis and D. Forster *et al.*, 2004. Bound exciton and donor–acceptor pair recombinations in ZnO. Phys. Stat. Sol., 241: 231-260. DOI: 10.1002/pssb.200301962

Minami, T., 2008. Substitution of transparent conducting oxide thin films for indium tin oxide transparent electrode applications. Thin Solid Films. 516: 1314-1321. DOI: 10.1016/j.tsf.2007.03.082

Mohanta, A., 2014. Effect of pressure and Al doping on structural and optical properties of ZnO nano-wires synthesized by chemical vapor deposition. J. Luminescence, 146: 470-474. DOI: 10.1016/j.jlumin.2013.10.028

Morkoç, H. and Ü. Özgür, 2009. Zinc Oxide: Fundamentals, materials and device technology. Wiley-VCH Verlag GmbH & Co. KGaA.

Mosbah, A. and M.S. Aida, 2012. Influence of deposition temperature on structural, optical and electrical properties of sputtered Al doped ZnO thin films. J. Alloys Compounds, 515: 149-153. DOI: 10.1016/j.jallcom.2011.11.113

N.L. Marana, S. Casassa, E. Longo and J.R. Sambrano *et al.*. Structural, electronic, vibrational and topological analysis of single-walled zinc oxide Nanotubes. J. Phys. Chem. C., 120: 6814-6823. DOI: 10.1021/acs.jpcc.5b11905

Nsimama, P.D. and M.E. Samiji, 2012. Electrical properties of DC reactive magnetron sputtered ZnO:Al films from optical spectra. Tanzania J. Sci., 38: 39-52.

Ong, K.S., J. Hu, R. Shrestha, F. Zhu and S.J. Chua, 2005. Flexible polymer light emitting devices using polymer-reinforced ultrathin glass. Thin Solid Films, 477: 32-37. DOI: 10.1016/j.tsf.2004.08.107.

Pankove, J.I., 1971. Optical Processes in Semiconductors. Dover Publications. Mineola NY.

Park, K.C., D.Y. Ma and K.H. Kim, 1997. The physical properties of Al-doped zinc oxide films prepared by RF magnetron sputtering. Thin Solid Films, 305: 201-209. DOI: 10.1016/S0040-6090(97)00215-0

Park, S.H., H.M. Kim, B.R. Rhee, E.Y. Ko and S.H. Shon *et al.*, 2001. Effects of oxygen concentration on characteristics of RF-Sputtered In2O3-ZnO thin films. Japanese J. Applied Phys., 40: 1429-1430.

Peres, M.A.B., 2007. Caracterização Óptica de amostras de ZnO. [Dissertation]. Aveiro: Universidade de Aveiro.

Pla, J., M. Tamasi, R. Rizzoli, M. Losurdo and E. Centurioni *et al.*, 2003. Optimization of ITO layers for applications in a-Siyc-Si heterojunction solar cells. Thin Solid Films, 425: 185-192. DOI: 10.1016/S0040-6090(02)01143-4

Rahmane, S., M.S. Aida, M.A. Djouadi and N. Barreauc 2015. Effects of thickness variation on properties of ZnO:Al thin films grown by RF magnetron sputtering deposition. Superlattices Microstructures, 79: 148-155. DOI: 10.1016/j.spmi.2014.12.001

Sahu, D.R. and J.L. Huang, 2006. High quality transparent conductive ZnO/Ag/ZnO multilayer films depo-sited at room temperature. Thin Solid Films. 515: 876-879. DOI: 10.1016/j.tsf.2006.07.049

Song, S., J. Jang, Y. Ji, S. Park and T.W. Kim *et al.*, 2013. Twistable nonvolatile organic resistive memory devices. Organic Electronics, 14: 2087-2092. DOI: 10.1016/j.orgel.2013.05.003

Sundaram, K.B. and A. Khan, 1997. Characterization and optimization of zinc oxide films by r.f. magnetron sputtering. Thin Solid Films. 295: 87-91. DOI: 10.1016/S0040-6090(96)09274-7

Tang, G., H. Liu and W. Zhang, 2013. The variation of optical band gap for ZnO:In films prepared by sol-gel technique. Advances in Mat. Scie. Eng., 2013: 1-4. DOI: 10.1155/2013/348601

Tohsophon, T., N. Wattanasupinyoa, B. Silskulsuka and N. Sirikulratb, 2011. Effect of aluminum and indium co-doping on zinc oxide films prepared by DC magnetron sputtering. Thin Solid Films, 520: 726-729. DOI: 10.1016/j.tsf.2011.06.079

Ushio, Y., M. Miyayama and H. Yanagida, 1994. Effects of interface states on gas-sensing properties of a CuO/ZnO thin-film heterojunction. Sens. Actuators B Chem., 17: 221-226. DOI: 10.1016/0925-4005(93)00878-3

Wang, T., Y. Liu, Q. Fang, M. Wu and X. Sun *et al.*, 2011. Low temperature synthesis wide optical band gap Al and (Al, Na) codoped ZnO films. Applied Surface Sci., 257: 2341-2345. DOI: 10.1016/j.apsusc.2010.09.100

Yoo, J., J. Lee, S. Kim, K. Yoon and J. Park *et al.*, 2005. High transmittance and low resistive ZnO:Al films for thin films solar cells. Thin Solid Films, 480-481: 213-217. DOI: 10.1016/j.tsf.2004.11.010

Yu, P. and M. Cardona, 2010. Fundamentals of Semiconductors. Springer. Heidelberg, pp: 775.

Yu, X.H., J. Ma and F. Ji, 2005. Effects of sputtering power on the properties of ZnO: Ga films deposited by r.f. magnetron-sputtering at low temperature. J. Crystal Growth, 274: 474-479. DOI: 10.1016/j.jcrysgro.2004.10.03

Zhang, X.T., Y.C. Liu, Z.Z. Zhi, J.Y. Zhang and Y.M. Lu *et al.*, 2002. Temperature dependence of excitonic luminescence from nanocrystalline ZnO films. J. Luminescence, 99: 149-154. DOI: 10.1016/S0022-2313(02)00331-9